Hindawi
Advances in Meteorology
Volume 2023, Article ID 1939528, 21 pages
https://doi.org/10.1155/2023/1939528

Research Article

Spatiotemporal Variability and Trends in Rainfall and Temperature in South Ethiopia: Implications for Climate Change Adaptations in Rural Communities

Daniel Dalle, Yisak Gecho, and Sisay Belay Bedeke

RDAE, Wolaita Sodo University, P.O. Box 138, Wolaita Sodo, Ethiopia

Correspondence should be addressed to Daniel Dalle; danieldalle258@gmail.com

Received 6 April 2023; Revised 9 September 2023; Accepted 11 September 2023; Published 25 September 2023

Academic Editor: Antonio Donateo

Climate change is an environmental challenge for rural communities that rely heavily on rainwater-based agriculture. The main goal of this study is to investigate spatiotemporal variability and trends in rainfall and temperature in southern Ethiopia. Extreme temperature and rainfall indices were computed using the ClimPACT2 software. The detection and quantification of trends in rainfall and temperature extremes were analyzed using a nonparametric modified Mann–Kendall (MMK) test and Sen's slope estimator. Results indicated that the mean annual rainfall has a declining trend at Boditi School and Mayokote stations with a statistically significant amount at magnitudes of 0.02 mm and 0.04 mm, respectively. The highest average monthly rainfall in the catchment was observed in the months of April, May, June, July, and August up to maximum rainfall of 117.50 mm, 177.43 mm, and 228.84 mm in Bilate Tena, Boditi, and Mayakote stations, respectively. On a seasonal scale, rainfall in Bilate Tena station was highly variable in all months, ranging from 49.54% to 126.92%, and three seasons except spring which showed moderate variation at 40.65%. In addition, the three locations over the catchment exhibited varied drought signs such as severe ($1.28 < \text{SRA} < 1.65$) and extreme drought ($\text{SRA} > 1.65$). The temperature indices, on the other hand, exhibited a warming trend over the catchment which was observed through an increased annual number of warm days (TX90p) and warm nights (TN90p) ranges from 0.274 to 6.03 and 0.274 to 3.16, respectively. The annual maximum value of the daily maximum temperature (TXx) ranges from 30.10 to 33.76°C in the three agroecological zones and showed low, medium, and high values in Dega, Woyna Dega, and Kola agroecologies, while the annual maximum value of the daily minimum temperature (TNx) ranged between 17 and 17.44°C at Dega and Kola, respectively. Therefore, based on trends in rainfall variability and persistent temperature rise, appropriate adaptation strategies should be adopted.

1. Introduction

Climate change is one of the global environmental changes which closely relates to the agricultural sector. Over the past few decades, the global climate has shown unprecedented change and continues to change in the future at an unparalleled rate [1, 2]. According to the latest report of the Intergovernmental Panel on Climate Change [3], the global average annual surface temperature has increased by 0.3 to 0.6°C since the late 19th century and is expected to increase by 1.0 to 3.5°C over the next 100 years. Nowadays, changes in the climate are recognized as one of the greatest environmental challenges of our time, which calls for a concerted effort by the international community to develop diverse adaptation and mitigation plans.

Climate change is a global threat causing severe, cross-sectoral, long-lasting, and, in some cases, irreversible impacts on agriculture [2]. However, the countries of the world do not withstand equally in front of climate change challenges. Climate change is leading to changes in the frequency, intensity, spatial extent, and time scale of extreme climate conditions, which can lead to unprecedented extreme events [4–7]. Low-income and fragile countries, including Ethiopia, are heavily dependent on rainwater-based agriculture, which is highly sensitive to climate change and has been hardest hit [8].

Among developing countries, Africa has several climate change hotspots, where the physical and environmental impacts of climate change cross with a large number of poor and vulnerable communities [9, 10]. The IPCC Assessment Report Six (AR6) states that sub-Saharan Africa is still experiencing a warming trend, with an average rate of change of roughly +0.3°C/decade from 1991 to 2021, compared to +0.2°C/decade from 1961 to 1990, 0.04°C/decade between 1931 and 1960, and +0.08°C/decade from 1901 to 1930 [11]. On the other hand, rainfall in the area varies greatly over both space and time due to a variety of complicated topographical factors and circulation patterns. Climate change adversity coupled with low adaptive capacity poses unanticipated threats to the majority of people in Africa, which affects the most vulnerable people by increasing food insecurity, population displacement, stress on water resources, and disease outbreaks [12–14].

As confirmed by previous studies, climate change in Ethiopia is fast-tracking and will lead to wide-ranging shifts in climatic conditions [15, 16]. The country's long-term climate data show that Ethiopia's climate, especially the distribution of rainfall and temperature, which has been relatively static for many years, has become very dynamic and unpredictable [17–19]. According to a report by the World Bank Group, over the past decades, the temperature in Ethiopia has increased by about 0.2°C per decade, while the average annual temperature is 22.6°C, with monthly temperatures ranging from 20.9°C to 23.9°C [19]. Despite the fact that the general trend for rainfall is still quite consistent when compared to the yearly average [20], there is a significant amount of variation in rainfall throughout both time and space. The average annual rainfall in Ethiopia is 815.8 mm, with a range from 0 mm to more than 4,000 mm per year [2]. This illustrates a high degree of regional variability and fluctuation over time.

The global climate model (GCM) predicts that the national average annual temperature will increase by 3.1°C by 2060 and 5.1°C by 2090, and rainfall will decrease from the annual average of 2.04 mm/day (1961–1990) to 1.97 mm/day (2070–2099).

Along with predicted rainfall, the future temperature change is one of the most important indicators of ongoing global climate change [21]. Changes in temperature, which cause alterations in rainfall patterns, are important for water resource management and water-related natural hazards [22].

In Ethiopia, several studies have assessed the variations in rainfall and temperature over a wide range of geographic areas and time scales [23–28]. Despite the fact that these studies offered an important foundation for understanding climate trends and variability, the majority of the previous studies were limited to data from a few selected meteorological stations. The regional weather stations have encountered a number of difficulties when attempting to acquire data, including low data quality (discontinuous data), lack of availability and accessibility, and unevenly distributed stations [29, 30]. Instead of station-based temperature and rainfall data, which can be obtained from local weather stations along with the satellite-based data, which can be downloaded from the Coordinated Regional Climate Downscaling Experiment (CORDEX) Africa programs. Using station-based data and household surveys at the national and subnational levels, other research studies have looked at the relationship between long-term trends in climate parameters; however, these studies may not fully describe the situation at the local level [23, 26–28].

The local level climate analysis on which this study is centered focused on the seasonal rainfall variability, including onset, cessation, and length of the growing season, and extreme events such as drought statistics generated for both long and short rainy seasons, rather than long-term trends, provides helpful insights into the current trajectory of various climate variables, particularly on shorter-term planning horizons. To characterize and comprehend the present and past climatic conditions, a detailed climate study at a higher temporal and spatial resolution is necessary. This will make it possible to offer data that will correctly guide the creation of programs for adaptation and mitigation. This type of research is, therefore, topical and appropriate for identifying regional and local patterns of climate change, developing treatments, and disseminating useful information about climate adversity.

Detecting area-specific spatiotemporal trends in meteorological time series is important for understanding the evidence and effects of climate change adversity across the country. Thus, our study investigates spatiotemporal variation and trends in daily, monthly, and yearly rainfall and temperature (maximum, minimum, and mean values) in the Wolaita zone, southern Ethiopia, for the year 1990–2021. In order to achieve the goal, the local level rainfall (annual, seasonal, and daily) as well as the daily maximum and minimum temperatures was hypothesized to be neither regularly distributed nor independent of the mean and standard deviation. This study is, therefore, very crucial to understand the spatial and temporal variations of climate change within a study area and its effect on farmers life. The study will also help to monitor and design natural resources management systems, such as environmental planning, land use planning, water resources planning, and irrigation planning while implementing sustainable agricultural development in the area.

2. Materials and Methods

2.1. Area under Study. The study area is situated in Wolaita zone which is one of the administrative areas of the Southern Nations, Nationalities, and Peoples Regional State (SNNPR) of Ethiopia. This zone is located 390 km southwest of the country's capital, Addis Ababa, along the main road from Shashamane to Arba Minch [29]. Figure 1 depicts the study area, Wolaita zone, which is astronomically positioned between 6.4°–7.1°N latitude and 37.4°–38.2°E longitude.

Wolaita zone covers a total area of 4,511.7 km^2 and is structured with 16 districts and 6 towns. Among the 16 districts of the Wolaita zone, this study was conducted on

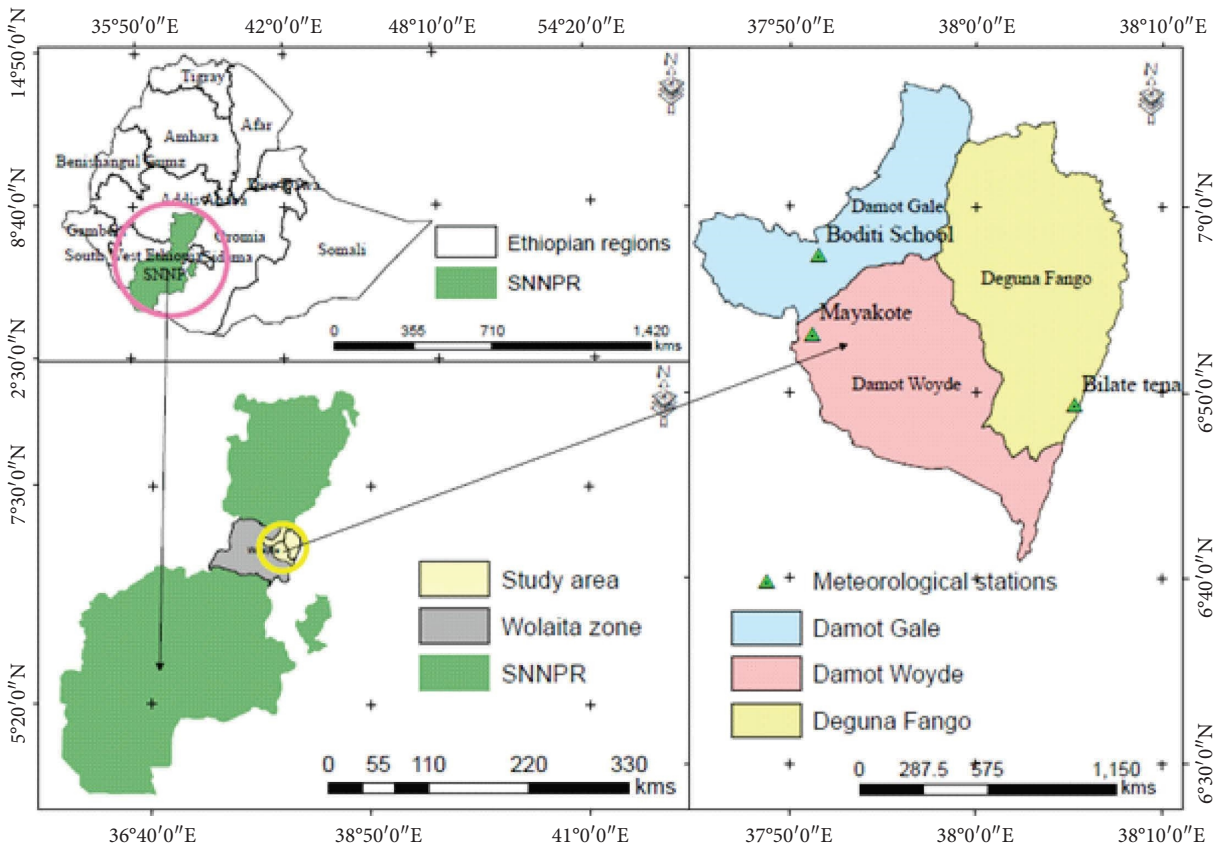

Figure 1: Map of the study area.

three sample areas under the Bilate Wolaita subwatershed, which are the main hotspot areas of the zone in terms of climate change extremes, food security, and land degradation [5]. The selection criteria for the study district were the predominant agroecology of the districts, the presence of meteorological stations, and agroecological location.

According to Ethiopia's classification of agroecological zones, the region is mostly characterized by mid-highland agroecology (1500–2300 m.a.s.l.). As per Ethiopia's traditional agroecological classifications, the study area is divided into three zones, with Woyna Dega making up the majority of the overall area at around 56%; the remaining 35% and 9% are referred to as Kola and Dega, respectively [30] (Table 1). The study extracted three meteorology stations based on the Ethiopian traditional AEZ grouping approach by employing latitude and longitude, elevation, and patterns of rainfall and temperature to represent the alpine vegetated zone known as "Dega," the temperate zone known as "Woyna Dega," and the hot zone known as "Kola" agroecological zones (AEZs), respectively.

It was quite challenging to forecast the patterns of rainfall and temperature in the study area. However, according to the Wolaita Zone Plan Department's annual report, the study area has two main rainy seasons: the long rainy season (Belg), which lasts from February to May, and the short rainy season (Kiremt), which lasts from June to September. According to the authors in [16], in the Wolaita zone, the average annual maximum and minimum temperatures range from 31.4°C to 15.2°C, while the zone's total mean annual rainfall ranges from 1000 mm to 1270 mm, with August often having the highest rainfall records. As a result, the climate change extremes severely affected the study area, particularly for people whose livelihoods heavily depend on subsistence agriculture.

2.2. Input Data Sources and Types

2.2.1. The Existing Data from Three Selected Meteorological Stations. To represent variation over space and time, three meteorological stations' recent records of daily rainfall and temperature data from 1990 to 2021 were used. The time series data for the chosen stations were supplied by the Ethiopian National Meteorological Agency, which is in task of gathering and studying meteorological data on a countrywide scale. As station-based data alone has low data quality and measurement mistakes in terms of consistency and precision [16, 30], this study used integrated quality-controlled station data from the national observatory network with locally calibrated satellite data. Due to the small number of stations, regional variability of the agroecology, and data gaps, better spatiotemporal climatological information is urgently needed to support climate services and related decision-making processes. To find mistakes and outliers, manual and automated data checks were also carried out.

Table 1: The study area's chosen meteorological stations with their annual average rainfall (mm) and temperatures (°C) from 1990 to 2021 years of observed data points in each gauging station.

Stations	Lat (N)	Long (E)	Elev (m)	Annual Avg. RF (mm)	Annual Avg. T_{max} (°C)	Annual Avg. T_{min} (°C)	AEZ	% of data availability
Boditi School at Damot Gale	6.57	37.51	2043	1237.64	20.09	15.24	Dega	97
Mayokote at Damot Woyde	6.58	37.58	2121	1514.28	22.39	18.84	W/Dega	97
Bilate Tena at Duguna Fango	6.92	38.12	1361	840.5	24.68	19.2	Kola	96

Source: own construction (2022) based on [31].

2.2.2. Climate Model Datasets Used. In the form of NetCDF (Network Common Data Form), downscaled rainfall and temperature data for the years 1976 to 2100 were obtained based on grid resolutions over all Coordinated Regional Climate Downscaling Experiment Africa programs for the RCPs. By utilizing many regional climate models (RCMs) throughout various domains around the world, including Africa, CORDEX carries a novel and distinct set of climate projections [32]. All RCMs simulate the fundamental climatic variables, including daily precipitation, maximum (T_{max}), and minimum (T_{min}) surface air temperatures; however, biases, including data irregularities, outliers, and missing values, exist across the models, making bias correction necessary before using the climate data for any analysis.

Four regional climatic models, namely, the Regional Atmospheric Climate Model Version 22 (RACMO22T), Rossby Center Atmospheric Version 4 (RCA4), Regional Model (REMO2009), and Community for Limited-Area Climate Modeling (CCLM4), were used in this study in order to better describe the spatiotemporal characteristics of climate change extremes. However, there are many criteria by which a subset of models can be selected, for instance, based on the skill in reproducing past climate [33] and the range of projected climate changes [34]. Others have implemented automated algorithms based on the clustering of climate extreme indices to identify a representative subset of climate models. Therefore, no single climate model can capture the entire range of possibilities for all factors, regions, or seasons. Working with a restricted selection of models can result in inconsistencies in climate change signals [35]. The simplification of extremely complex atmospheric physics in GCMs results in intrinsic errors and uncertainties. Due to the correction of individual errors, they discovered that a multiple model ensemble was a better fit for the situation than individual GCMs [36].

The climate models chosen for this study were based on earlier research in the catchment that outperformed other climate models [37]. The previous knowledge of selecting climate models from multiple GCM-RCMs is better to limit the number of climate models. The hydrostatic RCA4 model, which can generate data with a variety of horizontal resolutions but only with 0.44 grid resolution, was employed in this study. The study also utilized the fifth-order upwind nonhydrostatic regional climate model, Climate Limited-Area Modeling Community Version 4 (CCLM4), which offers a more accurate representation of the spatiotemporal variability of precipitation and temperature [38]. The Regional Model (REMO2009), a three-dimensional hydrostatic atmospheric regional climate model developed by the Max Planck Institute of Meteorology, was also utilized [38]. Moreover, the Regional Atmospheric Climate Model Version 22 (RACMO22T), the hydrostatic KNMI regional climate model and the latest iteration of the RACMO2, was also used. Climate variables are simulated by all regional climate models, but their magnitudes vary. The climate models used in this study revealed variations in capturing the observed rainfall and temperature in previous studies [37]. The models utilized in this study had a grid resolution of 0.44 by 0.44.

2.3. Management of Data

2.3.1. Bias Correction of Climatic Variables. Bias correction was applied to reduce overestimation or underestimation of the mean of downscaled variables (i.e., temperature and precipitation). Bias correction factors were computed from the statistics of observed and historical variables. The power transformation/nonlinear method was used to correct both the mean and variance of precipitation [37].

(1) Precipitation. Prior to using the climatic data for analysis of each station, the bias correction for the temperature and precipitation data was performed. The CV and mean are both corrected using a power transformation approach. Using the formula given in [39], each daily precipitation amount P was converted to a proper P_* using the following equation:

$$P_* = \mathrm{aP}^b. \tag{1}$$

The parameters a and b were determined for every month of the year, including data from all years available.

(2) Temperature. When monthly mean values are included, this method is capable of perfectly adjusting climatic influence. For each station, the corrected daily temperature T_* is given as follows:

$$T_* = \overline{T}_{\mathrm{obs}} + \frac{\sigma T_{\mathrm{obs}}}{\sigma T_{\mathrm{rcm}}} * \left(T_{\mathrm{obs}} - \overline{T}_{\mathrm{obs}}\right) + \left(T_{\mathrm{obs}} - \overline{T}_{\mathrm{rcm}}\right), \tag{2}$$

where T_{obs} is the observed daily temperature from the National Meteorological Agency (NMA) dataset and T_{rcm} is the uncorrected daily temperature from RCP.

(i) Estimating and filling missing data: Inverse distance or weighting method is most commonly used for the estimation of missing precipitation [40–42]. Rainfall data of interpolation using inverse distance weighting (IDW) can obtain more accurate results [43–46]. The rainfall at a station was estimated as a weighted average of the observed rainfall at the neighboring stations. The weights are equal to the reciprocal of the distance or some power of the reciprocal of the distance of the estimator stations from the estimated stations.

$$P_{*=} \frac{\sum_{i=1}^{n}\left(p_i/Di^2\right)}{\sum_{i=1}^{n}\left(1/Di^2\right)}, \tag{3}$$

where P_* is the rainfall of the missing station, n is the number of index stations, and

$$D_i^2 = \left[\left(x - x_i\right)^2 + \left(y - y_i\right)^2\right], \tag{4}$$

where D_i is the distance between the estimator station and the estimated station. Then, the estimator station's coordinates are x and y, whereas the estimated station's coordinates are x_i and y_i. In order to test consistency for some stations, the nondimensional sign of rainfall data was computed by dividing monthly time series data by the average rainfall amount of the respective month which is calculated as follows (Figure 2):

$$p_i = 100 * \frac{\overline{p_i}}{\overline{p}}, \tag{5}$$

where p_i is the nondimensional value of rainfall for month i, $\overline{p_i}$ is the over monthly rainfall at the station i, and $\overline{p}$ is the over yearly rainfall of the station.

(ii) Checking consistency of the rainfall data: Inconsistency may result from the unreported shifting of the rain gauge in the gauging station. Double-mass curve analysis was used to adjust inconsistent data. The change in the regime of the curve of the inconsistency was adjusted by using the following equation (Figure 3):

$$P_a = \frac{b_a}{a_o} * \left(p_o\right), \tag{6}$$

where P_a is the adjusted precipitation, p_o is the observed precipitation, a_o is the slope of graph at time p_o is observed, and b_a is the slope of graph to which records are adjusted.

(iii) Accuracy of rainfall simulations from climate models: In this work, the outputs of the model simulation of rainfall data were assessed using statistical techniques such as P_{Bias}, RMSE, Correl, and coefficient of variation (CV). *Percent of bias* can be estimated by using the following equation:

$$P_{\text{Bias}} = \frac{\left(R_{\text{RCM}} - \overline{R}_{\text{obs}}\right)}{\overline{R}_{\text{RCM}}} * 100, \tag{7}$$

where P_{Bias} is the percent of bias; $\overline{R}_{\text{obs}}$ is the average observed rainfall data; R_{RCM} is the rainfall data over the catchment; and $\overline{R}_{\text{RCM}}$ is the average rainfall data.

The coefficient of variation (CV) can be estimated by using the following equation:

$$\text{CV} = \frac{\delta R}{\overline{R}} * 100, \tag{8}$$

where CV is the coefficient of variation in %; δ is the standard deviation; R is the rainfall over the catchment; and $\overline{R}$ is the average rainfall over the catchment.

The root mean square error of a model prediction with respect to the estimated variable R_{RCM} is defined as the square root of the mean squared error which is given as follows:

$$\text{RMSE} = \sqrt{\sum_{i=1}^{N} \frac{\left(R_{\text{RCM}} - R_{\text{obs}}\right)^2}{N}}, \tag{9}$$

where RMSE is the relative mean square error in mm year^{-1}; R_{RCM} is the rainfall data over the catchment; R_{obs} is the observed rainfall data over the catchment; and N is the number of years that rainfall observed. Correlation coefficient (Correl) can be estimated as follows:

$$\text{correl} = \frac{\sum^{ni=1} \left(R_{\text{obs}} - \overline{R}_{\text{obs}}\right)\left(R_{\text{RCM}} - \overline{R}_{\text{RCM}}\right)}{\sqrt{\left(\sum_{i=1}^{n}\left(R_{\text{obs}} - \overline{R}_{\text{obs}}\right)^2 \sum_{i=1}^{n}\left(R_{\text{RCM}} - \overline{R}_{\text{RCM}}\right)^2\right)}}, \tag{10}$$

where correl is the correlation coefficient (−); R_{RCM} is the rainfall data over the catchment; R_{obs} is the observed rainfall data over the catchment; n is the number of observations; $\overline{R}_{\text{obs}}$ is the average observed rainfall data; and $\overline{R}_{\text{RCM}}$ is the average rainfall data of the climate.

2.3.2. Data Analysis. When bias was corrected, the actual analysis of the climatic data was carried out using parametric and nonparametric trend tests, which measure the magnitude of the trends in the extremes of climate change. The R and R Studio software packages (version 4.2.2) were used for data analysis. Several actual climate data analysis techniques have been developed for the analysis of rainfall and temperature, often falling under the category of variability and trend analysis. The analysis of variability involves using the coefficient of variation (CV) and the percentage deviation from the mean (anomaly), while nonparametric MMK trend test along with Sen's slop estimator, which is more robust for trend detection in time series, was used [46, 47]. The following indices and tests were conducted to analyze the spatiotemporal variations in rainfall and temperature within the study area.

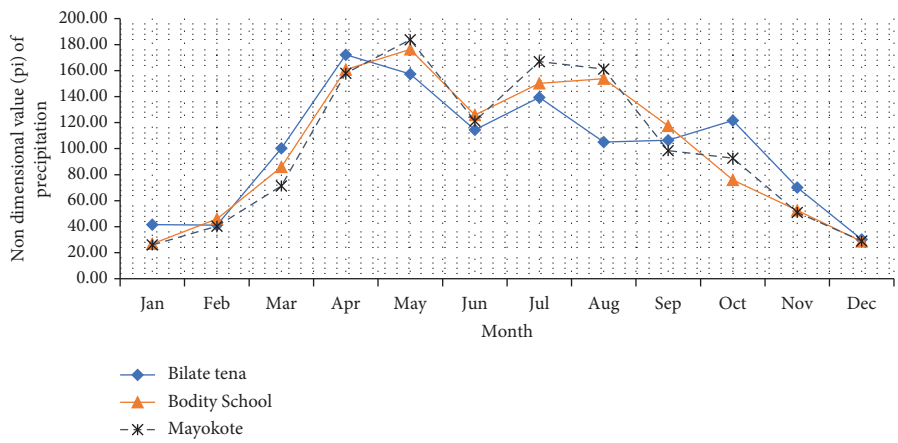

Figure 2: Rainfall homogeneity test.

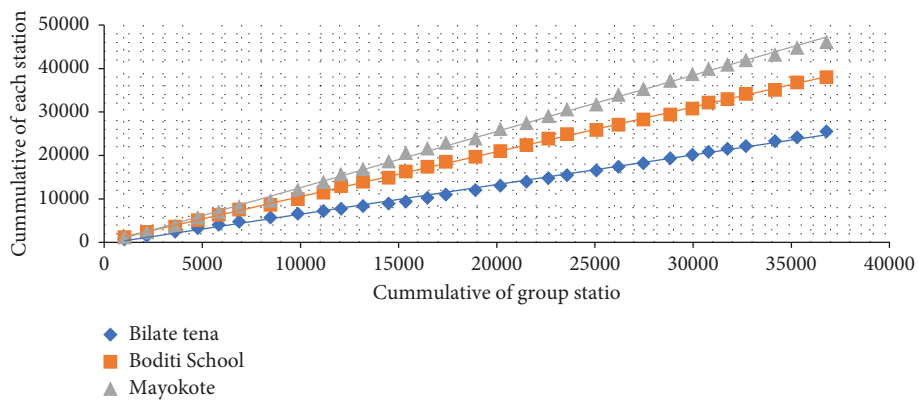

Figure 3: Double-mass curve analysis of rainfall.

(1) Analysis of Rainfall Variability

(i) The coefficient of variation in rainfall (CV): The coefficient of variation (CV) is a widely used technique to analyze interannual variability of rainfall computed as the ratio of the standard deviation to the mean value over the given period. The advantage of using the coefficient of variation (CV) is that it is a useful statistic for comparing the variability of one data series with another, even when the means are significantly different. However, CV is sensitive to small mean values and is unable to determine mean intervals, and it is not helpful to analyze the rainfall variability in a specific season. Despite this limitation, CV can be used to calculate the annual and interseason variability in rainfall. The greater variability is indicated by a higher coefficient of variation (CV), and vice versa:

$$\mathrm{CVx} = \frac{\sigma x}{\mu x}, \tag{11}$$

where CVx is the coefficient of variation for the given month or year, σx is the standard deviation for the given month or year, and μx is the mean value for the given month or year.

This study used the classification of CV in [48], which classifies CV values as less variable for values less than 0.20, moderately variable for values between 0.20 and 0.30, and highly variable for values greater than 0.30.

(ii) Standardized rainfall anomaly (SRA): SRA is commonly used as a simple index to characterize drought at different time scales or to identify abnormal wetness or dryness [49]. The standardized rainfall anomaly is calculated as the difference between long-term mean annual rainfall and observed annual rainfall to the ratio of standard deviation which is given as follows:

$$\mathrm{SRA} = \frac{p_t - p_m}{\sigma}, \tag{12}$$

where SRA is the standardized rainfall anomaly, p_t is the annual rainfall in the year, p_m is the long-term mean annual rainfall for the study period, and σ is the standard deviation of annual RF for the study period. The classification of drought severity given in [50], which is extreme drought ($\mathrm{SRA} > 1.65$), severe drought ($1.28 < \mathrm{SRA} < 1.65$), moderate drought ($-0.84 > \mathrm{SRA} > -1.28$), and no drought ($\mathrm{SRA} > -0.84$), was adopted in this study.

(iii) Standardized anomaly index (SAI): A standardized anomaly index (SAI) is a commonly used index for regional climate change analysis [51]. For each station, the series of mean annual temperature, mean annual minimum temperature, and average annual maximum temperature were analyzed to identify variations using a standardized anomaly index. Station temperature is expressed as a standardized departure x_i from the long-term mean and was calculated as follows:

$$x_i = \frac{r - r_i}{\sigma}, \tag{13}$$

where r is the mean temperature of the year, r_i is the long-term mean, and σ is the standard deviation of the annual mean temperature for the long term.

(iv) Extreme climate indices: One method to describe the intensity, duration, and frequency of climate extremes is to calculate climate indices based on daily time series of temperature and precipitation [52]. To better understand climate trends and extremes at various locations, the Expert Team on Climate Change Detection Monitoring Indices (ETCCDMI) has developed a number of indicators [53]. These indices were computed using R software interface that supports ClimPACT2, which is a Microsoft Excel-based tool that offers an intuitive software package for the computation of indices of climate extremes for monitoring and detecting climate change. The inverse distance weighted (IDW) interpolation technique, which is better at examining the geographical patterns of rainfall distribution, was used to explore the several extreme climate indicators geographically [54]. Under the assumption that the attribute value of an undetermined site is the weighted average of a known place, IDW achieves spatial interpolation. This is accomplished by applying the notion of distance balancing to assign values from known nearby places to the unknown site. The selected temperature and rainfall indicators used in this study are thoroughly summarized in Table 2.

(2) Trend Analysis of Rainfall and Temperature Indices

(i) Trend analysis using the MMK test: Several statistical tests exist to assess the significance of trends in time series. One of the most frequently used nonparametric trend tests is the Mann–Kendall trend test. The basic assumption of the Mann–Kendall trend test is that the data are independent and randomly ordered. However, as mentioned in [49], if persistence is not taken into consideration when using the Mann–Kendall (MK) test, the trend may not be accurate, which is true for the majority of climate data. To reduce serial correlation's impact on the MMK test, an improved form of the classic Mann–Kendall (MK) test called the modified Mann–Kendall (MMK) test was applied. The accuracy of the MMK test in terms of its empirical significance was found to be superior to the Mann–Kendall trend test without any loss of power. The MMK test can be used in conjunction with Sen's slope estimator to obtain the magnitude of the trend. For this purpose, a modified variance of S, designated as $\mathrm{Var}(S)^*$, was computed by using the following equation:

$$\mathrm{Var}(S)^* = V(S)\frac{n}{n^*}, \tag{14}$$

where n^* is the effective sample size and n/n^* is the ratio computed directly from the following equation:

$$\frac{n}{n^*} = 1 + \frac{2}{n(n-1)(n-1)} \times \sum_{\mathrm{k}=1}^{n-1} (n\mathrm{k} - \mathrm{k})(n-k-1)(n-k-2), \tag{15}$$

where "n" is the number of observations, "n^*" is the effective number of observation counts for autocorrelation, and "k" is the autocorrelation function for the rank of the observations.

(ii) Sen's slope estimator: One of the most common models for identifying linear trends is simple linear regression. But this approach needs to be predicated on residual normality [54, 55]. Thus, Sen's slope estimator is found to be a powerful tool to develop linear relationships. Sen's slope has an advantage over the regression slope, in that raw data series errors and outliers do not have much effect. In the nonparametric statistical tool, the magnitude of the trend that exists in the time series is estimated by Sen's slope estimator [56]. So, this study used Sen's slope to estimate the magnitude of the trends in the time series data in three selected stations. When the trend can be considered to be linear and equal, Sen's method can be utilized by using the following equation:

$$f(t) = Qt + \beta, \tag{16}$$

where $f(t)$ is a continuous monotonic increasing or decreasing function of time, Qt is the slope, and β is a constant.

The slopes of all data value pairs were calculated to get the slope estimate Q:

Table 2: Description of climate extreme indices [55].

Indices	Name description	Explanations	Units
Precipitation and temperature indices			
PRCPTOT	Annual total wet-day precipitation	Total annual precipitation in days ≥1 mm	mm
R95p	Very wet days	Precipitation totals annually from the days with daily RF > 95th percentile	mm
R99p	Extremely wet days	Annualized precipitation on days with a daily RF > 99th percentile	mm
R20mm	Number of very heavy precipitation days	Annual counts of days when rainfall ≥20 mm	days
R10mm	Number of heavy precipitation days	Annual counts of days when rainfall ≥10 mm	days
RX1day	Max 1-day precipitation amount	Annual maximum 1-day precipitation	mm
RX5day	Max 5-day precipitation amount	Annual maximum consecutive 5-day rainfall	mm
CWD	Consecutive wet days	Maximum number of consecutive days with RF ≥ 1 mm	days
CDD	Consecutive dry days	Maximum number of consecutive days with RF < 1 mm	days
SDII	Simple daily intensity index	Annual total rainfall when (PRCP ≥1 mm) divided by the number of wet days	mm/day
TX90p	Warm days	Percentage of days when T_{max} > 90th percentile	days
TN90p	Warm nights	Percentage of days when T_{min} > 90th percentile	days
TX10p	Cool days	Percentage of days when T_{max} < 10th percentile	days
TN10p	Cool night	Percentage of days when T_{min} < 10th percentile	days
TXx	Warmest day	Annual maximum value of the daily max temperature	°C
TNx	Warmest night	Annual maximum value of daily min temperature	°C
WSD1	Warm spell duration	Annual count of days with at least 6 consecutive days with T_{max} >90th percentile	days

$$Q_i = \frac{x_j - x_k}{j - k}, \quad \text{for } i = 1, \ldots, N, \tag{17}$$

where x_j and x_k are the data values at times j and k ($j > k$) and N is computed as follows:

$$N = \frac{n(n-1)}{2}, \tag{18}$$

where n is the number of periods, the N values of Q_i were ordered from smallest to largest, and the median slope or estimate of Sen's was calculated by using the following equation:

$$Q_{\text{med}} = \left\{ \begin{array}{ll} Q_{(N+1/2)} & \text{if} \quad N \text{ is odd,} \\ Q_{(N/2)} + Q_{(N+2/2)} & \text{if} \quad N \text{ is even.} \end{array} \right\}. \tag{19}$$

A positive value of Q_i indicates an increasing trend and a negative value of Q_i gives a decreasing trend in the time series [57].

3. Results and Discussion

3.1. RCM Model Performance Evaluation Result. Previously, for any impact assessment in the context of climate change, the accuracy of climate models in terms of statistical measures such as correlation (−) was used to assess the relationship between observed and modeled rainfall with a value of 1 and 0, suggesting a perfect linear relationship; bias indicates a systematic error in rainfall. A value of zero shows no systematic difference between simulated and observed rainfall amounts, whereas a large bias indicates that the RCM rainfall amount largely deviates from the observed rainfall amount. Positive bias indicates underestimation, while negative bias indicates overestimation. A root mean squared error (RMSE) number close to zero denotes the RCM model's optimal performance; the coefficient of variation (CV) and its ability to reproduce annual rainfall cycles must be evaluated. The observed catchment-averaged annual rainfall amount was 1185.28 mm year^{-1}. The accuracy of rainfall for the overlapping period from four GCM-RCMs (1990–2005) is shown in Table 3.

The rainfall in the catchment may not be accurately represented by all models. As shown in Table 4, some models slightly underestimate the observed rainfall, while others somewhat overestimate. The most precise estimating model should be used to calculate the observed rainfall in the catchments. The ensemble means performed the best in terms of bias (PBias = −0.0004%), whereas ICHEC-REMO2009 performs the worst (PBias = −0.003%). The value in PBias denotes that there was a systematic discrepancy between simulated and observed rainfall levels. The GCM-RCMs rainfall amount significantly differs from the observed rainfall amount, as shown by the high bias (PBias = −0.003%). The ensemble mean performed best in terms of CV (CV = 0.37%), while MPI-CCLM4 performed worst (CV = 0.75%). The ensemble mean also performs best (RMSE = 130.03 mm year^{-1}), while MPI-CCLM4 performed worst (RMSE = 194.5 mm·year^{-1}). However, the MPI-CCLM4 model performs best in terms of correlation coefficient (Correl = 0.43). CNRM-RCA4 has the worst performance (correl = −0.28). To estimate the observed mean annual rainfall quantity, this study used an ensemble mean, which performed 99.98% better than those four models.

Moreover, the monthly rainfall varies by a maximum of up to 173.93 mm from April to August. In the remaining months, the catchment received up to 48.59 mm in January, February, March, November, and December seeing the least amount of rainfall. Thus, RCMs model simulations reasonably reproduced the observed annual rainfall over the catchment after bias correction. The observed annual cycle of rainfall's amount and pattern were quite well captured.

3.2. Monthly and Seasonal Rainfall Variability

3.2.1. Rainfall Variability on a Monthly Basis. The catchment's mean monthly rainfall variability, standard deviation (SD), and coefficient of variation (CV) are provided in Table 4. Table 4 indicates that rainfall peaked at the Mayokote and Boditi School stations in May with 228.84 mm and 177.43 mm, respectively, while it peaked at the Bilate Tena stations in April with 117.50 mm. With the exception of spring, where there is a moderate variation, rainfall at Bilate Tena station fluctuates greatly throughout the year. Except for July, all other months at the Boditi School station had moderate rainfall variability, accounting for 28.59%, which ranges from 20% to 30%. Every month and season experienced a substantial variation in rainfall at Mayakote station.

3.2.2. Rainfall Variability on a Seasonal Basis. The catchment's seasonal variation in rainfall from 1990 to 2021 is presented in Table 4 and Figure 4. The Mayokote meteorology station recorded the highest summer rainfall variability with a magnitude of 44.21%, while the Bilate Tena and Boditi School meteorology stations varied with magnitudes of 39.17% and 23.77%, respectively. The Mayakote meteorology station in autumn (Belg) also recorded the highest rainfall variability (63.53%), followed by the station at Bilate Tena (47.79%) and Boditi School (37.59%). In the spring, rainfall varies by the magnitude of 48.17%, 40.65%, and 31.90% at the Mayakote Bilate Tena, and Boditi School meteorological stations, respectively. In the winter, rainfall varied considerably in all three stations with magnitudes ranging from 63.5% to 64.4%. Among the three stations, Mayokote exhibited the highest variability in all seasons and winter was the season with the very high variability recorded in all stations. Summer was found to be a season when high amounts of annual rainfall were received with a somewhat moderate variation. This result is consistent with recent findings by the authors in [23, 26, 46, 58, 59], which demonstrated that summer is primarily responsible for the highest annual rainfall received in different parts of the country with relatively low variation.

Figure 5 depicts the catchment's spatial distribution of seasonal rainfall, which varied from 23.77 to 64.38%, with 23.77 to 44.21% in the summer, 63.8 to 64.38% in the winter,

Table 3: Rainfall performance from four GCM-RCM models for overlapping periods (1990–2005).

	Annual avg. rainfall (mm)	P_{Bias} (%)	CV (%)	RMSE (mm year-1)	Correlation coefficient (–)
Observed	1185.28	—	0.48	—	—
MPI-CCLM4	1184.24	−0.002	0.75	194.53	0.43
ICHEC-RACMO2009	1184.30	−0.003	0.63	173.5	0.16
CNRM-RCA4	1185.29	0.002	0.63	175.66	−0.28
ICHEC-REMO2009	1185.30	0.001	0.62	174.14	−0.16
Ensemble mean	1185.27	−0.0004	0.37	130.03	0.20

Table 4: Data on the rainfall's coefficient of variation at three stations (1990–2021).

	Bilate Tena		CV (%)	Boditi School		CV (%)	Mayakote		CV (%)
	Mean (mm)	SD (mm)		Mean (mm)	SD (mm)		Mean (mm)	SD (mm)	
January	28.14	31.45	111.79	28.60	25.99	90.85	31.63	34.51	109.11
February	28.01	31.70	113.19	45.60	44.47	97.52	50.27	46.68	92.85
March	68.44	62.35	91.10	91.88	49.92	54.33	87.09	69.68	80.01
April	117.50	64.78	55.13	166.25	76.05	45.74	198.33	108.30	54.60
May	109.94	54.47	49.54	177.43	84.94	47.87	228.84	142.84	62.42
June	77.44	51.09	65.97	131.00	51.35	39.20	149.68	104.62	69.89
July	96.26	54.89	57.02	152.28	43.53	28.59	213.99	120.77	56.44
August	73.94	45.23	61.17	157.54	47.92	30.42	206.96	107.67	52.03
September	78.53	45.60	58.07	117.72	56.08	47.64	123.12	86.86	70.55
October	89.77	55.19	61.48	83.45	63.99	76.67	121.56	113.09	93.03
November	49.68	42.27	85.09	54.91	52.94	96.40	64.85	81.64	125.89
December	22.86	29.01	126.92	30.96	36.35	117.42	37.95	51.53	135.78
Summer	82.55	32.33	39.17	146.94	34.92	23.77	190.21	84.09	44.21
Autumn	72.66	34.73	47.79	85.36	32.09	37.59	103.18	65.55	63.53
Winter	26.34	16.81	63.84	35.05	22.57	64.38	39.95	25.58	64.02
Spring	98.62	40.09	40.65	145.19	46.32	31.90	171.42	82.57	48.17

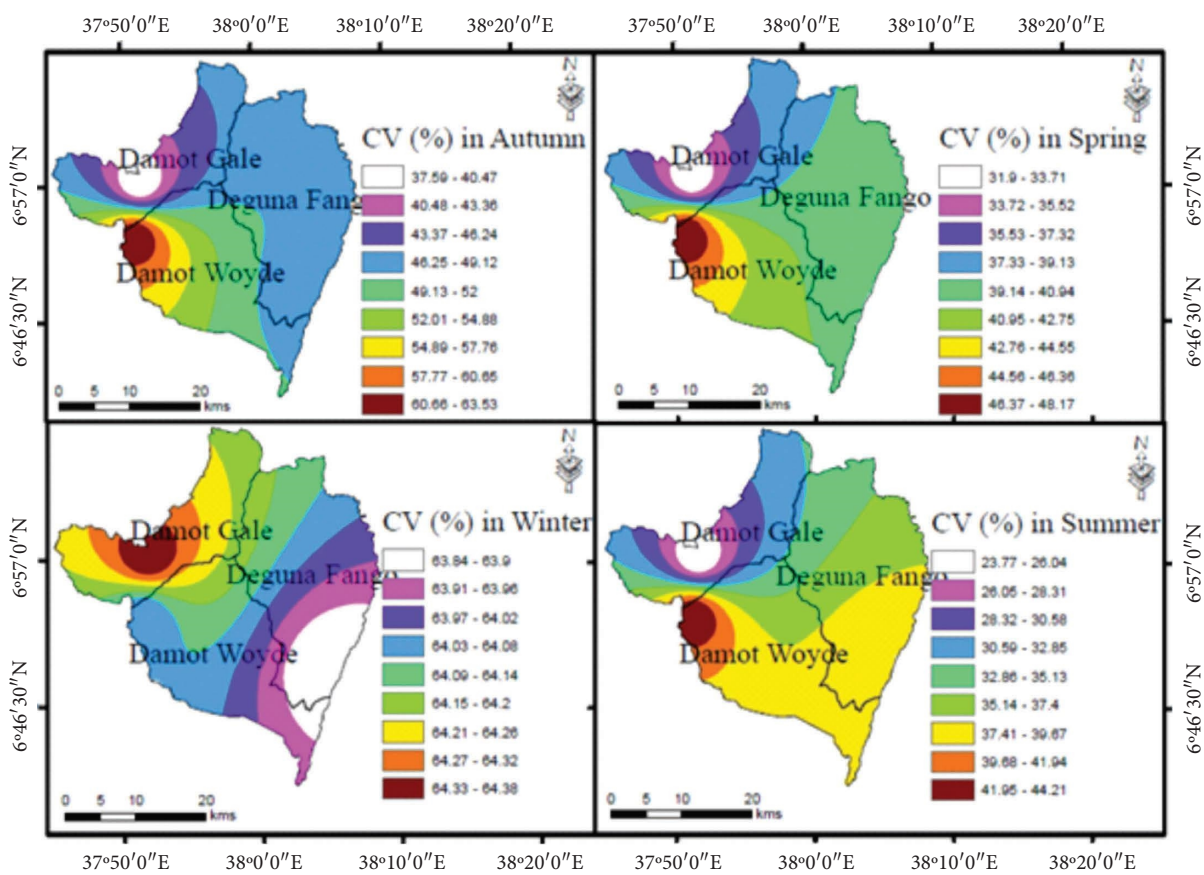

Figure 4: Spatial distribution of rainfall variability on a seasonal basis (1990–2021).

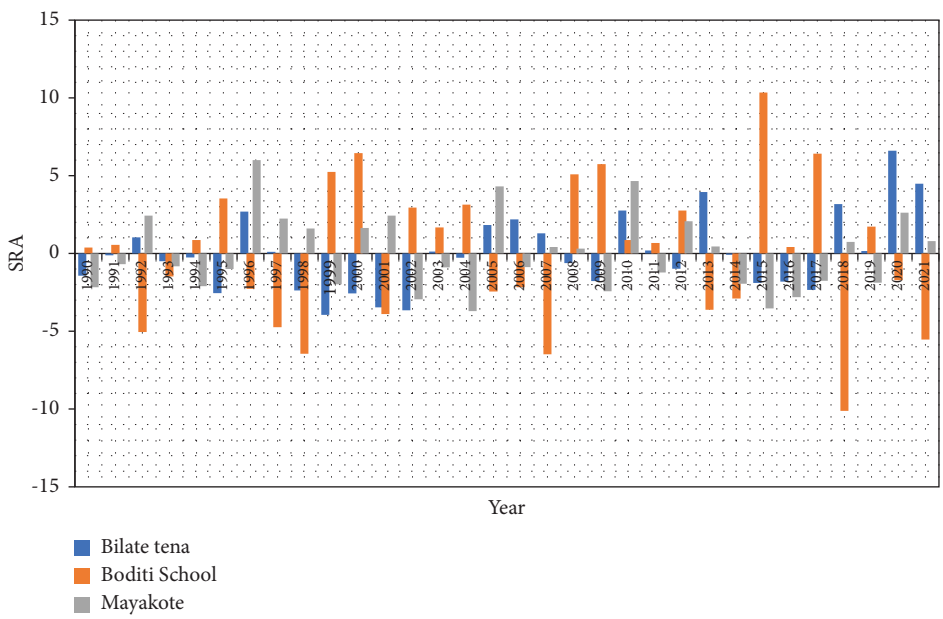

Figure 5: Anomaly of standardized rainfall over the catchment at the yearly base.

37.59 to 63.53% in the autumn, and 31.9 to 48.17% in the spring over the study period. Agroecologically, the summer rainfall varied within the same range in the Woyna Dega and Kola agroecologies (32.86 to 44.21%). In the same way, the winter rainfall varied between 63.84 and 64.2% in the Woyna Dega and Kola agroecologies. Autumn rainfall, however, varied substantially at different agro ecologies, with ranges of 46.25 and 49.12% in Kola, 49.19 to 63.53 in Woyna Dega, and 37.59 to 46.24% in Dega agroecologies. Agroecologically, spring rainfall in Dega, Kola, and Woyna Dega varied from 31.9 to 39.13%, 39.14 to 40.94%, and 40.94% to 48.17%, respectively. Generally, the Woyna Dega agroecology (Damote Woyde district) has demonstrated extremely high seasonal rainfall variability, followed by Kola (Duguna Fango district) and Dega (Damote Gale district), respectively.

In contrast to this result, the authors in [16, 31, 55] reported that the kola agroecology had significantly higher seasonal rainfall variability than the rest by taking elevation into account as one of the main determining variables for seasonal rainfall distribution. According to [60], a number of climatological factors, including the southerly/south westerly cross-equatorial moisture flow from the Southern Indian Ocean and the seasonal northward advance of the intertropical convergence zone that persisted over Ethiopia, govern the spatial distribution of seasonal rainfall in Ethiopia. In accordance with the findings of this study, the authors in [8, 24, 56, 61] showed that Woyna Dega agroecology had extremely high seasonal rainfall variability, whereas Kola agroecology had the highest relative to Dega agroecology. Consequently, the adaptive response to extreme climate event done in the area should be feasible with agroecological heterogeneity.

3.3. Standardized Rainfall Anomaly (SRA). Using the standardized rainfall anomaly (SRA) findings, a study of the yearly rainfall variability over each station is shown in (Figure 5). As shown in Figure 6, over the study period, 56.25% negative deviations from the norm to 43.75% positive deviations were observed at the Bilate Tena station, 43.75% negative anomalies compared to 56.25% positive anomalies at the Boditi School station, and 53.125% negative anomalies compared to 46.875% positive anomalies at the Mayakote station. Hence, in contrast to Bilate Tena and Mayokote stations, where the negative anomaly was dominant and substantial cooling was evident, Boditi School station exhibited the positive anomaly, demonstrating the persistence of the warming period over the years 1990–2021.

3.4. Standardized Anomaly Index (SAI). A popular index for analyzing local climate change is the standardized anomaly index (SAI) [51]. In this study, the standardized anomaly index (SAI) was used to characterize the distribution of temperature in the study area for the years 1990–2021. The study analyzed the series of mean annual temperature, mean annual minimum temperature, and average annual maximum temperature for each station. The final depiction of the outcome showed a cooling time where the long-term average prevails out and a warming phase when the long-term average dominates. As illustrated in Figure 6, the three stations showed the mixed signal of the standardized anomaly index (SAI) on an annual basis. The patterns of temperature anomalies showed a time when the below long-term average predominated (cooling) and a time when the above lasting average persisted (warming). The outcome revealed that the cooling phase started in 1990 and continued uninterruptedly through 2005. On the other hand, from 2006 to 2021, above-

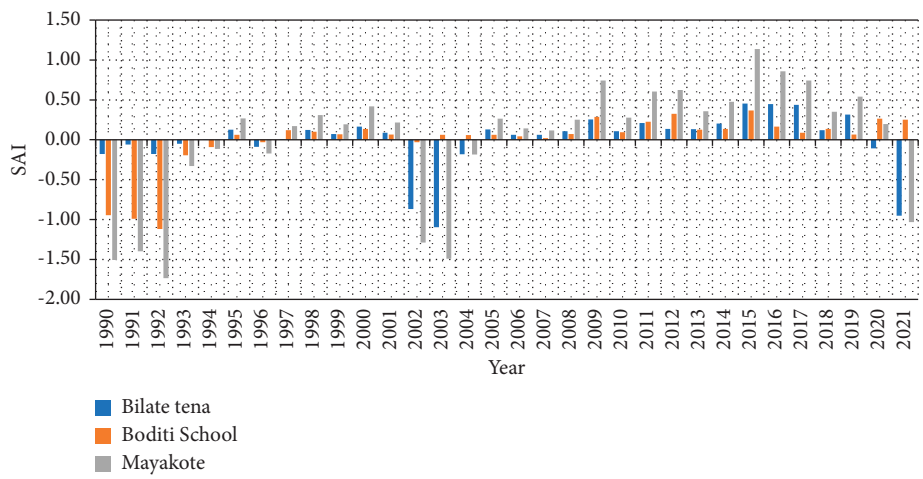

Figure 6: Standardized anomaly index (SAI) on an annual basis over the catchment.

average mean annual temperatures were recorded. With little breaks, temperatures rose gradually, and from 2006 to 2021, they were consistently above-average levels.

3.5. Temporal and Spatial Trends Examination of Rainfall

3.5.1. Rainfall Indices in terms of Intensity. As can be seen in Table 5, the modified Mann–Kendall's (MMK) trend test was used to examine the PRCPTOT, RX1day, RX5day, R95P, R99P, and SDII rainfall intensity indices for three stations (Bilate Tena, Boditi School, and Mayakote) throughout the period of 1990–2021. The trend in the annual total wet-day precipitation (PRCPTOT), annual maximum 1-day precipitation (RX1day), annual maximum 5-day precipitation (RX5day), very wet days (R95P), annual total precipitation on days when daily rainfall is greater than 99th percentile (R99p), and an index of the number of wet days (SDII) was observed for the Bilate Tena station to be increasing. On the days when daily precipitation exceeded the 99th percentile (R99p), the annual total precipitation was negligible. All rainfall intensity indices displayed a growing trend, with the exception of total yearly wet-day precipitation (PRCPTOT), which exhibited a barely dropping trend for the Boditi School station. At the Mayakote station, it was determined that the total yearly wet-day precipitation (PRCPTOT), very wet days (R95P), and number of wet days index (SDII) were all dropping at a 5% level whereas the annual maximum 1-day precipitation (RX1day) and the annual maximum 5-day precipitation (RX5day) had increased in Mayakote station. The details of each rainfall index are presented in Table 5.

Figure 7 illustrates the spatial distribution of rainfall intensity indices, which revealed that the total yearly wet-day precipitation (PRCPTOT) ranged from 1013 to 1412 mm and was found to be highest in the southwestern part of the catchment and lowest in the central and extreme northeastern parts. It was also found to be all rainfall indices except SDII, which have high rainfall intensity in the southwestern part of the catchments; others such as RX1day, RX5day, R99P, and SR95P have high rainfall intensity in the northeastern parts of the catchment. Agroecologically, the highest intensity was recorded in the Kola agroecology (Duguna Fango district), while the lowest intensity was recorded in the Dega agroecology (Damote Gale area), and Woyna Dega received the medium rainfall intensity.

In terms of the annual maximum 5-day precipitation (RX5day), the Kola and Woyna Dega agroecologies had the highest intensity (141–165 mm), while the Dega agroecology had the lowest intensity (88.8–140 mm). The Kola and Woyna Dega agro ecologies received the highest intensity (49 to 57 mm) of the annual maximum 1-day precipitation (RX1day), while the Dega agroecology recorded the lowest intensity (39 to 48 mm). Likewise, the Kola and Woyna Dega agroecologies experienced the maximum intensity (243–252 mm) of extremely wet days (R95P), with the lowest intensity recorded (232–242 mm) in Dega agroecology. In addition, the Dega, Woyna Dega, and Kola agroecologies were shown from lowest to highest in terms of annual total precipitation on days with daily rainfall over 99 percentiles (R99p), which ranged from 39.5 to 146 mm. However, the number of wet days index (SDII) was observed to be high in Dega, medium in Woyna Dega, and low in Kola agroecologies. The Dega agroecology displayed the lowest intensity, whereas the Kola and Woyna Dega agroecologies received the maximum intensity in all rainfall indices, with the exception of the number of wet days index (SDII). This result is consistent with the recent studies [16, 55, 56, 58], which identified that Kola agroecology has a higher rainfall intensity than Dega agroecology in terms of all rainfall intensity indices.

3.5.2. Rainfall Indices in terms of Frequency. Table 6 and Figure 8 present the statistical results of the temporal trends and spatial distribution of frequency indices composed of R10 mm, R20 mm, CWD, and CDD. The modified Mann–Kendall test-based rainfall frequency analysis displayed a significant positive trend in the number of days with substantial precipitation (R10 mm), the number of days with extremely substantial precipitation (R20 mm), and the number of consecutive dry days (CDD), but no trend in the number of days with consecutive wet days (CWD) for the catchment.

Table 5: MMK's trend statistics of rainfall intensity indices summary.

Modified MK statistics	SDII	RX5 day	RX1 day	R99p	R95p	PRECPTOT
Bilate station						
Corrected Zc	3.84	5.40	2.23	1.63	6.56	3.58
New *P* value	0.00	$6.5E-08$	0.03	0.10	0.00	0.00
N/N^*	0.15	0.12	0.06	0.24	0.08	0.24
Original Z	1.50	1.86	0.55	0.80	1.89	1.76
Old *P* value	0.13	0.06	0.58	0.43	0.05	0.07
Tau	0.18	0.23	0.07	0.09	0.23	0.22
Sen's slope	0.05	1.13	0.15	0	4.32	7.39
Old. variance	3802.66	3802.66	3801.66	3637.66	3802.66	3802.66
New. variance	587.25	452.89	231.61	868.66	317.66	924.67
Trend nature	Increasing	Increasing	Increasing	No trend	Increasing	Increasing
Trend significance	Significant	Significant	Significant	Not significant	Significant	Significant
Boditi station						
Corrected Zc	2.33278689	1.37	2.08	0.44	0.30	−0.52
New *P* value	0.02	0.17	0.04	0.65	0.76	0.59
N/N^*	0.09	0.17	0.11	0.13	0.07	0.11
Original Z	0.70	0.56	0.68	0.16	0.08	−0.17
Old *P* value	0.48	0.57	0.49	0.86	0.93	0.85
Tau	0.08	0.07	0.086	0.02	0.01	−0.02
Sen's slope	0.01	0.31	0.118	0	0.28	−0.36
Old. variance	3802.66	3802.66	3799.66	3675.66	3802.66	3802.66
New. variance	339.77	648.68	407.68	495.17	272.94	435.33
Trend nature	Increasing	Increasing	Increasing	No trend	Increasing	Decreasing
Trend significance	Significant	Not significant	Significant	Not significant	Not significant	Not significant
Mayakote station						
Corrected Zc	−1.78	0.13	1.68	0.45	−0.45	−1.06
New *P* value	0.07	0.89	0.09	0.64	0.65	0.28
N/N^*	0.09	0.38	0.29	0.12	0.28	0.10
Original Z	−0.53	0.08	0.90	0.15	−0.24	−0.34
Old *P* value	0.59	0.93	0.36	0.87	0.80	0.73
Tau	−0.06	0.01	0.11	0.02	−0.03	−0.04
Sen's slope	−0.03	0.09	0.28	0	−0.80	−3.10
Old. variance	3802.67	3802.66	3801.66	3213.33	3802.66	3802.66
New. variance	341.20	1480.44	1107.16	386.67	1094.02	391.08
Trend type	Decreasing	Increasing	Increasing	No trend	Decreasing	Decreasing
Trend significance	Not significant	Not significant	Not significant	Not significant	Not significant	Not significant

Except for consecutive wet days (CWD), which had no trend and hence have a Sen's slope of 0.00, the number of consecutive dry days (CDDs), heavy precipitation days (R10 mm), and very heavy precipitation days (R20 mm) all exhibited considerably rising trends for the Bilate tena station that was at Duguna Fango agroecological area. Consecutive dry days (CDDs) and consecutive wet days (CWDs) in Boditi School station showed significantly increasing trends; however, the increase in the number of days with heavy precipitation (R10 mm) showed a decreasing trend but was statistically insignificant. The trends in the number of extremely heavy precipitation days (R20 mm) in Boditi School station showed no trend. At Mayakote station, trends in the frequency of days with heavy precipitation (R10 mm) and very heavy precipitation (R20 mm) showed declining trends but were statistically insignificant. Both the consecutive dry days (CDDs) and the consecutive wet days (CWDs) at Mayakote station showed an upward trend, while the increase in the consecutive wet days (CWDs) is statistically insignificant (Table 6).

Figure 9 depicts the spatial distribution of rainfall frequency indices, with the Woyna Dega agroecology having the highest number of days with very heavy precipitation (R20 mm), the Kola agroecology having the fewest days, and the Dega agroecology having a medium number of days within the catchment. The quantity of days with a lot of rain (R10 mm), in catchments ranged from 33 to 38 days, with the Kola and Woyna Dega agroecologies recording the highest frequency and the Dega agroecology exhibiting the lowest frequency.

Continuous wet days (CWDs) ranged in length from 8 to 24 days in the watershed. Kola agroecology recorded the highest number of consecutive wet days (CWDs), while Dega agroecology recorded the fewest number of CWD and Woyna Dega agroecology had a medium number of CWD. The catchment's consecutive dry days (CDDs) ranged from 17 to 22 days, with Dega agroecology recording the highest number of days and Woyna Dega and Kola agroecology recording the lowest number of days. The rainfall frequency indices in Kola agroecology revealed a rising frequencies,

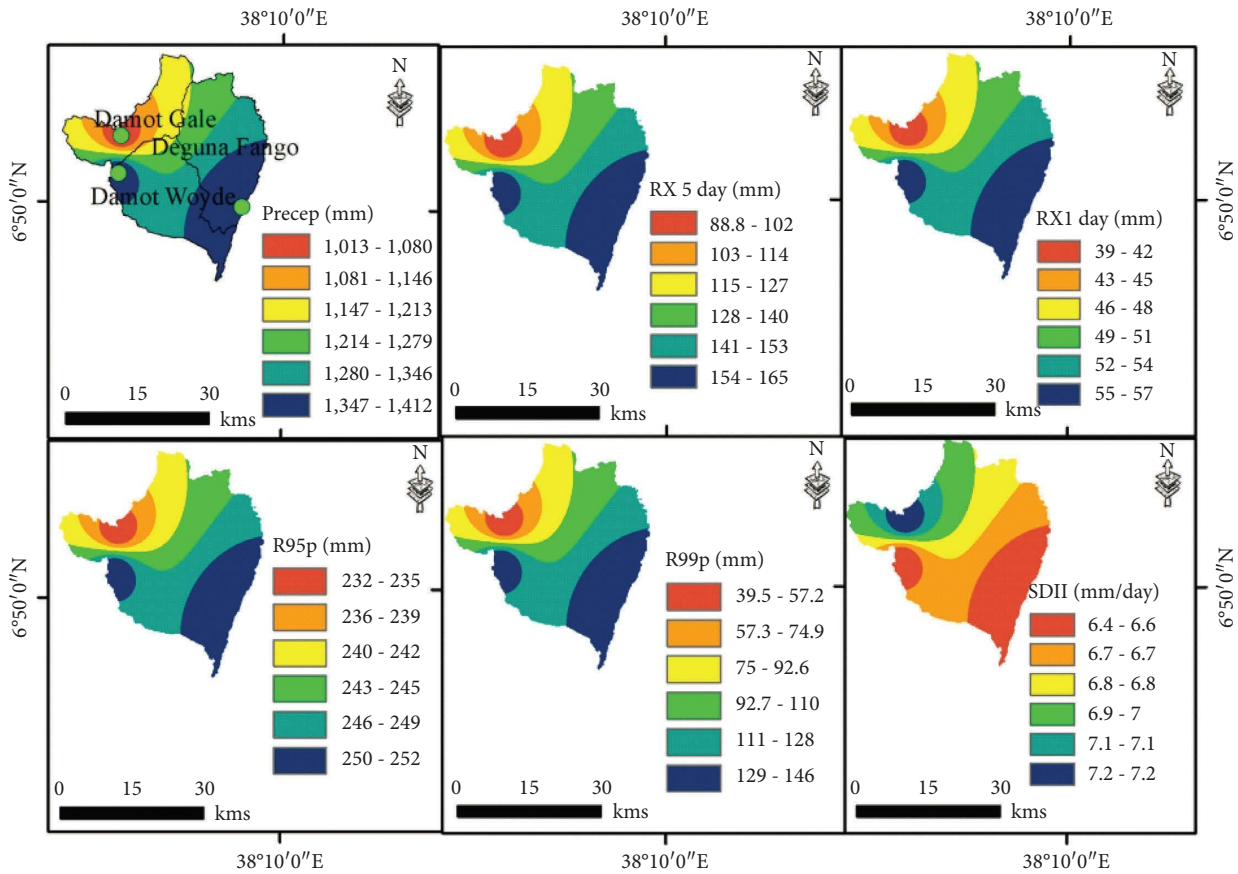

Figure 7: Annual extreme rainfall intensity indexes' spatial distribution.

Table 6: The modified Mann–Kendall's trend statistics of rainfall frequency indices.

Modified MK statistics	CDD	CWD	R20 mm	R10 mm
Bilate station				
Corrected Zc	2.26	1.12	4.58	3.26
New *P* value	0.02	0.26	$4.6E-06$	0.00
N/N^*	0.10	0.23	0.16	0.26
Original Z	0.74	0.54	1.83	1.67
Old *P* value	0.45	0.58	0.06	0.10
Tau	0.09	0.06	0.22	0.20
Sen's slope	0.32	0.00	0.17	0.22
Old. variance	3794.33	3678.67	3772.66	3749.66
New. variance	410.95	864.90	608.20	981.40
Trend type	Increasing	No trend	Increasing	Increasing
Trend significance	Significance	Not significance	Significance	Significance
Boditi School station				
Corrected Zc	3.05	1.98	0.24	−1.20
New *P* value	0.01	0.05	0.80	0.23
N/N^*	0.14	0.52	0.11	0.17
Original Z	1.17	1.42	0.08	−0.50
Old *P* value	0.24	0.15	0.93	0.61
Tau	0.14	0.17	0.01	−0.06
Sen's slope	0.27	0.04	0	−0.07
Old. variance	3786.33	3619	3766	3782.66
New. variance	556.43	1891.73	414.57	668.52
Trend type	Increasing	Increasing	No trend	Decreasing
Trend significance	Significance	Significance	Not significance	Not significance

Table 6: Continued.

Modified MK statistics	CDD	CWD	R20 mm	R10 mm
Mayakote station				
Corrected Zc	3.74	0.78	−2.16	−1.40
New *P* value	0.00	0.43	0.03	0.16
N/*N**	0.13	0.44	0.09	0.18
Original Z	1.37	0.52	−0.66	−0.60
Old *P* value	0.16	0.60	0.50	0.54
Tau	0.17	0.06	−0.08	−0.07
Sen's slope	0.65	0.03	−0.12	−0.12
Old. variance	3794.66	3758.33	3781.33	3787.33
New. variance	513.84	1648.88	358.80	694.59
Trend type	Increasing	Increasing	Decreasing	Decreasing
Trend significance	Significance	Not significance	Significance	Not significance

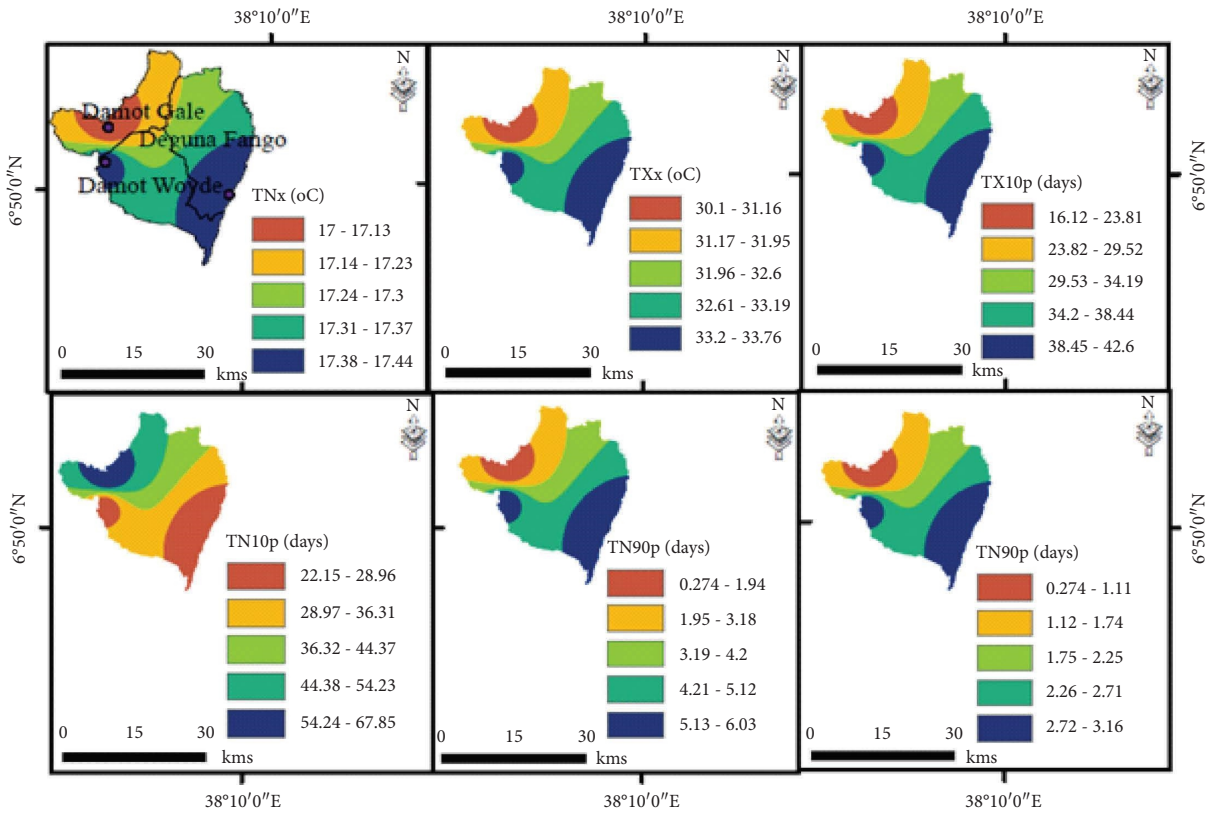

Figure 8: Spatial distribution of temperature indices.

with the exception of consecutive dry days (CDDs), which were high in Dega agroecology and supported by past studies [62]. However, conflicting results were found by the authors in [60, 62–64], and the disparity with these findings may be attributed to variations in the study period and place.

(1) Temperature Indices Trend Analysis. The temperature indices of the three stations represented the overall rising trend for the years 1990 to 2021, according to Table 7 analysis of the modified Mann–Kendall's (MMK) trend test results. The findings showed that for three stations across the study period, the annual warm day (TX90p), warm night (TN90p), the annual maximum value of the daily minimum temperature or warmest night (TNx), and the annual maximum value of the daily maximum temperature (TXx) were all observed to be increasing. However, the trends for cool days (TX10P) and cool nights (TN10P) varied across the three stations over the study period. In contrast to the trend for cool nights (TN10p), which exhibited decreasing trends in all three stations with statistically significant only at Bilate Tena stations, the trend for cool days (TX10p) increases in Boditi School stations and decreases in both Mayokote and Bilate Tena stations, which was consistent with the recent findings [8, 23, 25, 30, 65] (Table 8).

As illustrated in Figure 8, all the temperature indices in the catchment varied spatially over the study period. The catchment's annual warm days (TX90p) varied spatially, ranging from 0.27 to 6.027 days, with more heating in the

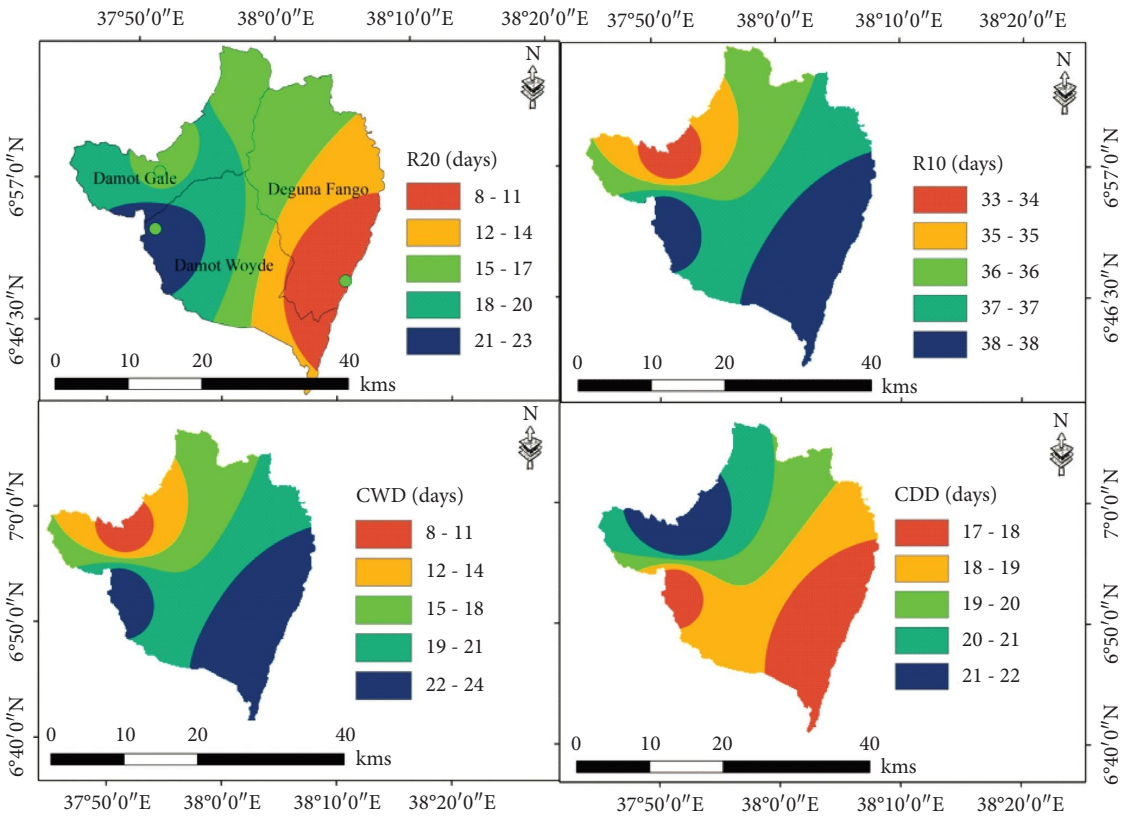

Figure 9: Spatial distribution of rainfall indices in terms of frequency.

southerly part of the study area. Likewise, warm nights (TN90p), which ranged from 0.274 to 3.163 days, showed long days of heating at night in the southern place of the catchments. Over the study period, the frequency of cool nights (TN10p), which shows 22.148 to 67.853 days, decreased in the southeast of the catchment and increased in the northeast and the opposit is true for cold days (TX10p). The frequency of the warmest nights (TNx) and warmest days (TXx) showed increasing and decreasing trends in the southern and northern parts of the catchment, respectively.

Three agroecologies recorded the warmest night (TNx), with Kola and Woyna Dega having the highest warm night and Dega agroecology recording the lowest. Regarding the warmest days (TXx), Kola and Woyna Dega agroecologies recorded the maximum warmest days, whereas Dega agroecology reported the minimum. Similarly, the cool days (TX10p) varied agro ecologically, with the maximum at Kola and Woyna Dega agroecologies and the minimum at Dega agroecology. However, the reverse is true for cool nights (TN10p) which showed maximum cool night in Dega and minimum cool night in Kola and Woyna Dega agroecologies. Consistent with annual warm nights (TN90p), warm days (TX90p) varied agro ecologically, with maximum in Kola and Woyna Dega agroecologies and a low or minimum at Dega agroecology. This was consistent with past research results that showed a general trend of rising warm and falling cold extremes in the studied area [8, 16, 62, 66]. The observed fluctuations in extreme temperature could be attributed to climate change, which is mostly brought about by human activities like deforestation and greenhouse gas emissions from industry and agriculture [7, 8].

3.6. Climate Change Projections in the Study Area. The projections of climate change over two decades under the RCP4.5 and RCP8.5 scenarios compared with the baseline (1976–2005) are presented in Table 7. In the first two decades, the mean annual temperature is likely to increase to 0.86°C and 0.85°C under RCP4.5 and RCP8.5 scenarios between the years 2020 and 2039, respectively. Under the RCP4.5 and RCP8.5 scenarios, the annual average temperature will rise to a maximum of 0.91°C and 0.94°C, respectively, from 2040 to 2059. Under the RCP4.5 and RCP8.5 scenarios, the temperature is projected to rise by 0.91°C and 1.04°C from 2060 to 2079 and by 0.95°C and 1.17°C from 2080 to 2099 in comparison to the baseline period (1976–2005). However, the average annual temperature will increase by more than 1°C between 2060 and 2079 and 2080 and 2099 years under the RCP8.5 high emission scenario. This is consistent with the study outputs of [67–74]. Moreover, the projections of future climate change indicate that continued GHGs emissions will lead to further warming and changes in climate conditions which share the truth [2, 7, 11, 23].

Table 7: Projected changes in the climate under low emission (RCP4.5) and high emission (RCP8.5) scenarios in comparison with the baseline period (1976–2005).

Climatic variables	2020–2039		2040–2059		2060–2079		2080–2099	
	RCP4.5	RCP8.5	RCP4.5	RCP8.5	RCP4.5	RCP8.5	RCP4.5	RCP8.5
Annual average temperature change	+0.74 to 0.86	+0.71 to 0.85	+0.77 to 0.91	+0.83 to 0.94	+0.82 to 0.91	+0.94 to 1.04	+0.84 to 0.95	+1.04 to 1.17
Annual precipitation changes	−31.52 to 24.31	−34.16 to 28.06	−30.00 to 22.83	−37.87 to 12.41	−27.03 to 28.21	−38.52 to 9.23	−28.52 to 21.37	−58.75 to 12.31

Table 8: The modified Mann–Kendall's trend statistics of temperature indices.

Modified MK statistics	TX90p	TN90p	TX10p	TN10p	TXx	TNx
Bilate station						
Corrected Zc	2.17	3.57	−2.45	−10.08	4.47	2.54
New *P* value	0.03	0.00	0.01	$6.4E-24$	$7.7E-06$	0.01
N/N^*	0.37	0.48	0.25	0.18	0.16	0.15
Original Z	1.32	2.48	−1.24	−4.32	1.79	0.99
Old *P* value	0.18	0.01	0.21	$1.49E-05$	0.07	0.32
Tau	0.16	0.31	−0.15	−0.54	0.22	0.12
Sen's slope	0.24	0.24	−0.04	−0.37	0.04	0.02
Old. variance	3801.66	3802.66	3800.66	3802.66	3774.33	3780
New. variance	1431.59	1832.41	986.25	700.915	605.04	574.57
Trend type	Increasing	Increasing	Decreasing	Decreasing	Increasing	Increasing
Trend significance	Significant	Significant	Significant	Significant	Significant	Significant
Boditi School station						
Corrected Zc	7.39	6.03	0.75	−0.86	8.47	4.78
New *P* value	$1.4E-13$	$1.6E-09$	0.45	0.38	$2.3E-17$	$1.70E-06$
N/N^*	0.52	0.95	0.93	1.77	0.11	0.54
Original Z	5.33	5.88	0.72	−1.15	2.85	3.54
Old *P* value	$9.5E-08$	$3.9E-09$	0.46	0.24	0.00	0.00
Tau	0.66	0.73	0.09	−0.14	0.35	0.43
Sen's slope	0.71	0.64	0.08	−0.02	0.08	0.08
Old. variance	3802.66	3802.66	3802.66	3796	3752.66	3740.66
New. variance	1979.14	3619.40	3560.12	6749.91	426.21	2056.15
Trend type	Increasing	Increasing	Increasing	Decreasing	Increasing	Increasing
Trend significance	Significance	Significant	Not significance	Not significance	Significance	Significant
Mayakote station						
Corrected Zc	7.96	6.50	−1.61	−3.25	2.38	3.26
New *P* value	$1.7E-15$	$7.96E-11$	0.10	0.00	0.01	0.00
N/N^*	0.21	0.38	0.30	1.60	0.42	0.34
Original Z	3.68	4.05	−0.89	−4.11	1.55	1.91
Old *P* value	0.00	$5.0E-05$	0.37	$3.9E-05$	0.11	0.05
Tau	0.45	0.50	−0.11	−0.51	0.19	0.23
Sen's slope	0.54	0.56	−0.11	−0.13	0.04	0.03
Old. variance	3802.66	3801.66	3802.66	3784	3797.66	3795
New. variance	813.13	1478.68	1154.71	6058.75	1616.83	1308.62
Trend type	Increasing	Increasing	Decreasing	Decreasing	Increasing	Increasing
Trend significance	Significant	Significant	Not significant	Significant	Significant	Significant

The annual precipitation change is anticipated to increase to values of 24.31% and 28.06%, 22.83% and 12.41%, 28.21 and 9.23%, and 21.37% and 12.31, respectively, between the years 2020–2039, 2040–2059, 2060–2079, and 2080–2099. The variation in annual precipitation will increase more in the medium term and decrease in the far future under both RCPs. Temperature will increase consistently in the study area, but precipitation shows varying changes across the catchment as discussed [19, 67–74].

4. Conclusions

This study investigated space-time trends and variations in duration, intensity, and frequency of climate extremes using different meteorological indices at three stations in the Wolaita zone southern Ethiopia, for the period 1990–2021. The results revealed that over the study period, the main climatic variables, temperature and rainfall, changed both spatially and temporally in the study area. The finding further indicated that maximum and minimum temperatures showed high spatiotemporal anomaly with overall significant warming, but on an annual basis, the three stations showed a mixed signal of anomaly. Similarly, the results of the modified Mann–Kendall's trend test also supported the notion that nearly all temperature indices from the three stations during the research period represented the overall upward trend both during the day and at night. The catchment's spatial distribution of seasonal rainfall varied from 23.77 to 64.38%, with 23.77 to 44.21% in the summer, 63.8 to 64.38% in the winter, 37.59 to 63.53% in the autumn, and 31.9 to 48.17% in the spring over the study period. Agroecologically, the summer rainfall varied within the same range in the Woyna Dega and Kola agroecologies (32.86 to 44.21%). In the same way, the winter rainfall varied between 63.84 and 64.2% in the Woyna Dega and Kola agroecologies. Autumn rainfall, however, varied substantially at different agro ecologies, with ranges of 46.25 and 49.12% in Kola, 49.19 to 63.53 in Woyna Dega, and 37.59 to 46.24% in Dega agroecologies. Agroecologically, spring rainfall in Dega, Kola, and Woyna Dega varied from 31.9 to

39.13%, 39.14 to 40.94%, and 40.94% to 48.17%, respectively. Generally, the Woyna Dega agroecology (Damote Woyde district) has demonstrated extremely high seasonal rainfall variability, followed by Kola (Duguna Fango district) and Dega (Damote Gale district), respectively. The modified Mann–Kendall test also revealed that while there was no trend for consecutive wet days (CWDs) in the watershed, there were positive trends in the number of heavy precipitation days, the number of very heavy precipitation days, and consecutive dry days across the study period.

The projections from the selected model outputs under both scenarios revealed a significant increase in temperature over the study period, compared to the baseline period (1976–2005). The average annual temperature will rise by more than 1°C under a high emission scenario. However, the variation in annual precipitation will increase more in the medium term and decrease in the far future under both emission scenarios. Warming temperatures and unpredictable rainfall timing and distribution make their choice of management practices more difficult and directly affect the productivity of rain-fed agriculture and the livelihoods of rural farmers. In order to address these challenges, farmers, agricultural researchers, and extension experts must work together. They also need to localize climate trend analysis to identify the similarities and contrasts in the climatic extremes that farmers experience in various agroecological settings. The study also recommended the establishment of timely and accurate climatic information, such as seasonal forecasts and early warning systems, which can be used as a reference for decision-making, planning, and policy implications on agriculture and climate change adaptation. Thus, this study urges policy-driven initiatives to convert climate-sensitive livelihood systems into climate-smart alternatives, thereby overcoming the difficulties associated with the effects of extreme climate change. The limited number of rainfall gauging stations was used in this study that conveys less information. Therefore, it is strongly advised that weather station quality and quantity be enhanced in order to increase the model's performance by include a sufficient number of highly effective hydrometeorological stations.

Data Availability

All the datasets used to support the findings of the study are available from the corresponding author upon request.

Conflicts of Interest

The authors declare that there are no conflicts of interest among the authors regarding the publication of this paper.

Acknowledgments

The authors would like to acknowledge all data providers, namely, MoWIEE (Ministry of Water Irrigation and Energy of Ethiopia) and NMAE (National Meteorology Agency of Ethiopia), for providing the required data. The authors are also thankful to Wolaita Sodo University, who has provided all logistical support in conducting the research work.

References

[1] M. Asmamaw, S. T. Mereta, and A. Ambelu, "Exploring households' resilience to climate change-induced shocks using Climate Resilience Index in Dinki watershed, central highlands of Ethiopia," *PLoS One*, vol. 14, no. 7, 2019.

[2] Wmo, *Global Annual to Decadal Climate Update*, Wmo, Geneva, Switzerland, 2021.

[3] IPCC, "Summary for Policymakers: Climate Change 2022 Impacts, Adaptation and Vulnerability_Working Group II Contribution to the Sixth Assessment Report of the Intergovernamental Panel on Climate Change," 2022, https://www.ipcc.ch/report/ar6/wg2/.

[4] S. I. Seneviratne, "Changes in climate extremes and their impacts on the natural physical environment," in *Managing the Risks of Extreme Events and Disasters to Advance Climate Change Adaptation.A Special Report of Working Groups I and II of the Intergovernmental Panel on Cli*, Cambridge University Press, New York, NY, USA, 2012.

[5] B. Esayas, B. Simane, E. Teferi, V. Ongoma, and N. Tefera, "Climate variability and farmers' perception in southern Ethiopia," *Advances in Meteorology*, vol. 2019, Article ID 7341465, 19 pages, 2019.

[6] R. J. T. Klein, "Adaptation Opportunities, Constraints, and Limits," Climate Change 2014: Impacts, Adaptation. Vulnerability Part A Glob. Sect. Asp.," 2015, https://www.ipcc.ch/site/assets/uploads/2018/02/WGIIAR5-Chap16_FINAL.pdf.

[7] Wagaye and A. Endalew, "Climatology and weather forecasting temperature and rainfall trends in North Eastern Ethiopia," *Climatol. Weather Forecast OPEN*, vol. 8, no. 3, pp. 1–6, 2020.

[8] D. M. Moges and H. G. Bhat, "Climate change and its implications for rainfed agriculture in Ethiopia," *Journal of Water and Climate Change*, vol. 12, no. 4, pp. 1229–1244, 2021.

[9] I. Niang, "Africa. In: Climate Change 2014: Impacts, Adaptation, and Vulnerability," *Contribution of Working Group II to the Fifth Assessment Report of the Intergovernmental Panel on Climate Change*, pp. 1199–1266, Cambridge University Press, New York, NY, USA, 2015.

[10] O. Laban, *Climate Variability and Change in Africa: A Review of Potential Impacts on Terrestrial Water Resources*, vol. 334, IAHS-AISH Publication, Wallingford, UK, 2009.

[11] Ipcc, "Bulletin of the Chinese academy of sciences," *IPCC AR6 WGI*, vol. 34, no. 2, p. F0003, 2021.

[12] C. Stadtbäumer, B. Ruesink, and S. Gronau, "Climate change scenarios in Zambia: modeling farmers' adaptation," *Agriculture and Food Security*, vol. 11, no. 1, pp. 52–16, 2022.

[13] C. Perez, "How resilient are farming households and communities to a changing climate in Africa? A gender-based perspective," *Global Environmental Change*, vol. 34, pp. 95–107, 2015.

[14] A. Dale, C. Fant, K. Strzepek, M. Lickley, and S. Solomon, "Climate model uncertainty in impact assessments for agriculture: a multi-ensemble case study on maize in sub-Saharan Africa," *Earth's Future*, vol. 5, no. 3, pp. 337–353, 2017.

[15] J. Birkmann, "Framing vulnerability, risk and societal responses: the MOVE framework," *Natural Hazards*, vol. 67, no. 2, pp. 193–211, 2013.

[16] B. Esayas, "Temperature and rainfall trends in North Eastern Ethiopia," *Advances in Meteorology*, vol. 10, no. 2, pp. 1–16, 2020.

[17] Usaid, "Climate Risk Profile Ethiopia," 2016, https://www.preventionweb.net/publication/climate-risk-country-profile-ethiopia#~text=Ethiopia%20is%20exposed%20to%20numerous,and%20impact%20since%20the%201970s.

[18] M. Gezie, "Farmer's response to climate change and variability in Ethiopia: a review," *Cogent Food and Agriculture*, vol. 5, no. 1, Article ID 1613770, 2019.

[19] The World Bank Group, *Climate Risk Profile: Ethiopia*, The World Bank Group, Washington, DC, USA, 2020.

[20] M. Legesse, K. Mohammed, T. Yisihak, M. Arja, and H. Bogale, "Effect of climate change on water availability in Bilate catchment," *Southern Ethiopia*, vol. 3, pp. 86–99, 2022.

[21] A. A. Mekonen and A. B. Berlie, "Rural households' livelihood vulnerability to climate variability and extremes: a livelihood zone-based approach in the Northeastern Highlands of Ethiopia," *Ecological Processing*, vol. 10, no. 1, p. 55, 2021.

[22] M. Abbas, L. Zhao, and Y. Wang, "Perspective impact on water environment and hydrological regime owing to climate change: a review," *Hydrology*, vol. 9, no. 11, p. 203, 2022.

[23] A. Mihiretu, E. N. Okoyo, and T. Lemma, "Small holder farmers' perception and response mechanisms to climate change: lesson from Tekeze lowland goat and sorghum livelihood zone, Ethiopia," *Cogent Food and Agriculture*, vol. 6, no. 1, Article ID 1763647, 2020.

[24] F. Destaw and M. M. Fenta, "Climate change adaptation strategies and their predictors amongst rural farmers in Ambassel district, Northern Ethiopia," *Jamba (Potchefstroom, South Africa)*, vol. 13, no. 1, pp. 974–1011, 2021.

[25] D. Etana, D. J. R. M. Snelder, C. F. A. van Wesenbeeck, and T. de Cock Buning, "Trends of climate change and variability in three agro-ecological settings in central Ethiopia: contrasts of meteorological data and farmers' perceptions," *Climate*, vol. 8, no. 11, pp. 121–127, 2020.

[26] A. D. Assamnew and G. M. Tsidu, "The performance of regional climate models driven by various general circulation models in reproducing observed rainfall over East Africa," *Theoretical and Applied Climatology*, vol. 142, no. 3–4, pp. 1169–1189, 2020.

[27] A. Belay, J. W. Recha, T. Woldeamanuel, and J. F. Morton, "Smallholder farmers' adaptation to climate change and determinants of their adaptation decisions in the Central Rift Valley of Ethiopia," *Agriculture and Food Security*, vol. 6, no. 1, pp. 24–13, 2017.

[28] G. Gitima, A. Legesse, and D. Biru, "Assessing the impacts of climate variability on rural households in agricultural land through the application of livelihood vulnerability index," *Geosfera Indonesia*, vol. 6, no. 1, p. 96, 2021.

[29] Y. Gecho, G. Ayele, T. Lemma, and D. Alemu, "Livelihood strategies and food security of rural households in," *Development Ctry Studies*, vol. 4, no. 14, pp. 123–136, 2014.

[30] T. M. Olango, B. Tesfaye, M. Catellani, and M. E. Pè, "Indigenous knowledge, use and on-farm management of enset (Ensete ventricosum (Welw.) Cheesman) diversity in Wolaita, Southern Ethiopia," *Journal of Ethnobiology and Ethnomedicine*, vol. 10, no. 1, pp. 41–18, 2014.

[31] B. T. Lambe and S. Kundapura, "Analysis of meteorological variability and tendency over Bilate basin of Rift Valley Lakes basins in Ethiopia," *Arabian Journal of Geosciences*, vol. 14, no. 23, p. 2692, 2021.

[32] A. Meque and B. J. Abiodun, "Simulating the link between ENSO and summer drought in Southern Africa using regional climate models," *Climate Dynamics*, vol. 44, no. 7–8, pp. 1881–1900, 2015.

[33] D. W. Pierce, T. P. Barnett, B. D. Santer, and P. J. Gleckler, "Selecting global climate models for regional climate change studies," *Proceedings of the National Academy of Sciences of the United States of America*, vol. 106, no. 21, pp. 8441–8446, 2009.

[34] C. F. McSweeney, R. G. Jones, R. W. Lee, and D. P. Rowell, "Selecting CMIP5 GCMs for downscaling over multiple regions," *Climate Dynamics*, vol. 44, no. 11–12, pp. 3237–3260, 2015.

[35] M. Turco, A. Sanna, S. Herrera, M. C. Llasat, and J. M. Gutiérrez, "Large biases and inconsistent climate change signals in ENSEMBLES regional projections," *Climatic Change*, vol. 120, no. 4, pp. 859–869, 2013.

[36] D. A. Hughes, S. Mantel, and T. Mohobane, "An assessment of the skill of downscaled GCM outputs in simulating historical patterns of rainfall variability in South Africa," *Hydrology Research*, vol. 45, no. 1, pp. 134–147, 2014.

[37] T. Y. Ukumo, A. Abebe, T. K. Lohani, and M. L. Edamo, "Flood hazard Mapping and Analysis under Climate Change Using Hydro-Dynamic Model and RCPs Emission Scenario in Woybo River Catchment of Ethiopia," *World Journal of Engineering*, vol. 20, 2022.

[38] R. Zentek and G. Heinemann, "Verification of the regional atmospheric model CCLM v5.0 with conventional data and lidar measurements in Antarctica," *Geoscientific Model Development*, vol. 13, no. 4, pp. 1809–1825, 2020.

[39] R. Leander and T. A. Buishand, "Resampling of regional climate model output for the simulation of extreme river flows," *Journal of Hydrology*, vol. 332, no. 3–4, pp. 487–496, 2007.

[40] S. Ly, C. Charles, and A. Degré, "Geostatistical interpolation of daily rainfall at catchment scale: the use of several variogram models in the Ourthe and Ambleve catchments, Belgium," *Hydrology and Earth System Sciences*, vol. 15, no. 7, pp. 2259–2274, 2011.

[41] M. A. D. Ukumo, T. Yisihak, and Muluneh Legesse Edamo, "Evaluating water availability under changing climate scenarios in the Woybo catchment," *Journal of Water and Climate Change*, vol. 13, no. 11, pp. 4130–4149, 2022.

[42] S. M. Boltana, D. W. Bekele, T. Y. Ukumo, and T. K. Lohani, "Evaluation of irrigation scheduling to maximize tomato production using comparative assessment of soil moisture and evapotranspiration in restricted irrigated regions," *Cogent Food and Agriculture*, vol. 9, no. 1, 2023.

[43] F. Chen, F. Chen, and C. Liu, "Estimation of the Spatial Rainfall Distribution Using Inverse Distance Weighting (IDW) in the Middle of Taiwan," *Paddy and Water Environment*, vol. 10, 2014.

[44] M. Legesse, E. Samuel, D. Hatiye, and T. T. Minda, "Flood inundation and risk mapping under climate change scenarios in the lower Bilate catchment, Ethiopia," *Natural Hazards*, vol. 118, 2023.

[45] K. B. Mirani, M. A. Ayele, T. K. Lohani, and T. Y. Ukumo, "Evaluation of hydropower generation and reservoir operation under climate change from kesem reservoir, Ethiopia," *Advances in Meteorology*, vol. 2022, Article ID 3336257, 14 pages, 2022.

[46] T. Y. Ukumo, T. K. Lohani, M. L. Edamo, M. A. Alaro, M. A. Ayele, and H. B. Borko, "Application of regional climatic models to assess the performance evaluation of changes on flood frequency in woybo," *Advances in Civil Engineering*, vol. 2022, Article ID 3351375, 16 pages, 2022.

[47] T. Bekuma, G. Mamo, and A. Regassa, "Variability and trends of climate in east Wollega zone, Western Ethiopia," *IOP Conference Series: Earth and Environmental Science*, vol. 1016, no. 1, Article ID 012032, 2022.

[48] A. Gebremicheal, "Analysis of seasonal rainfall variability for agricultural water resource management in southern region, Ethiopia soil and water conservation view project," *Insitu*

moisture conservation View project, vol. 4, no. 11, pp. 56–80, 2014.

[49] K. Koudahe, A. J. Kayode, A. O. Samson, A. A. Adebola, and K. Djaman, "Trend analysis in standardized precipitation index and standardized anomaly index in the context of climate change in southern Togo," *Atmospheric and Climate Sciences*, vol. 7, no. 04, pp. 401–423, 2017.

[50] C. T. Agnew and A. Chappell, "Drought in the Sahel," *GeoJournal*, vol. 48, pp. 299–311, 2000.

[51] J. S. Babatolu and R. T. Akinnubi, "Surface temperature anomalies in the river Niger basin development authority areas, Nigeria," *Atmospheric and Climate Sciences*, vol. 03, no. 04, pp. 532–537, 2013.

[52] T. C. Peterson, "Recent changes in climate extremes in the Caribbean region," *Journal of Geophysical Research*, vol. 107, pp. 1–9, 2002.

[53] G. E. Soro, D. Noufé, T. Albert, G. Bi, and B. Shorohou, "Trend Analysis for Extreme Rainfall at Sub-daily and Daily Timescales in Côte D ' Ivoire," *MDPI*, vol. 4, 2016.

[54] G. T. Oyerinde, A. Attogouinon, and A. A. Afouda, *Over the Ou É M É River Basin*, Benin, 2017.

[55] E. W. M. Lucas, "Trends in climate extreme indices assessed in the Xingu river basin- Brazilian Amazon," *Weather and Climate Extremes*, vol. 31, Article ID 100306, 2021.

[56] R. Fernandes and S. G Leblanc, "Parametric (modified least squares) and non-parametric (Theil-Sen) linear regressions for predicting biophysical parameters in the presence of measurement errors," *Remote Sensing of Environment*, vol. 95, no. 3, pp. 303–316, 2005.

[57] T. Teyso and A. Anjulo, "Spatio-temporal variability and trends of rainfall and temperature over gamo gofa zone, Ethiopia," *Journal of Scientific Research and Reports*, vol. 12, no. 2, pp. 1–11, 2016.

[58] W. B. Abegaz and E. A. Abera, "Temperature and rainfall trends in North Eastern Ethiopia," *J Clim. Weather Forecast 8262*, vol. 8, no. 262, pp. 1–6, 2020.

[59] D. Assefa and M. Mengistu, "Time Series Trend and Variability Analysis of Temperature and Rainfall in West Shewa Zone of Oromia, Ethiopia," *Natural Resources Management*, 2021.

[60] Z. T. Segele and P. J. Lamb, "Characterization and variability of Kiremt rainy season over Ethiopia," *Meteorology and Atmospheric Physics*, vol. 89, no. 1–4, pp. 153–180, 2005.

[61] J. Ali Mohammed, T. Gashaw, G. Worku Tefera, Y. T. Dile, A. W. Worqlul, and S. Addisu, "Changes in observed rainfall and temperature extremes in the upper blue nile basin of Ethiopia," *Weather and Climate Extremes*, vol. 37, Article ID 100468, 2021.

[62] M. A. Degefu and W. Bewket, "Trends and spatial patterns of drought incidence in the Omo-Ghibe River Basin, Ethiopia," *Geografiska Annaler- Series A: Physical Geography*, vol. 97, no. 2, pp. 395–414, 2015.

[63] T. M. Weldegerima, T. T. Zeleke, B. S. Birhanu, B. F. Zaitchik, and Z. A. Fetene, "Analysis of rainfall trends and its relationship with SST signals in the lake tana basin, Ethiopia," *Advances in Meteorology*, vol. 2018, Article ID 5869010, 10 pages, 2018.

[64] G. Tesso, B. Emana, and M. Ketema, "A TIME SERIES ANALYSIS OF CLIMATE VARIABILITY AND ITS IMPACTS ON FOOD PRODUCTION IN NORTH SHEWA ZONE IN Ethiopia Climate change (CC) manifest in the form of temperature increases, changes in precipitation and sea level rise, and the intensification of," *African Crop Science Journal*, vol. 20, pp. 261–274, 2012.

[65] W. T. Hailesilassie, T. Ayenew, and S. Tekleab, "Analysing trends and spatio-temporal variability of precipitation in the main central rift valley lakes basin, Ethiopia," *Environmental and Earth Sciences Research Journal*, vol. 8, no. 1, pp. 37–47, 2021.

[66] L. B. Chang'a, A. L. Kijazi, P. M. Luhunga, H. K. Ng'ongolo, and H. I. Mtongor, "Spatial and temporal analysis of rainfall and temperature extreme indices in Tanzania," *Atmospheric and Climate Sciences*, vol. 07, no. 04, pp. 525–539, 2017.

[67] S. Chakraborty, R. P. Pandey, U. C. Chaube, and S. K. Mishra, "Trend and variability analysis of rainfall series at Seonath River Basin, Chhattisgarh (India)," *International Journal of Applied Science and Engineering Research*, vol. 2, no. 4, pp. 425–434, 2013.

[68] D. Ademe, B. F. Zaitchik, K. Tesfaye, B. Simane, G. Alemayehu, and E. Adgo, "Climate trends and variability at adaptation scale: patterns and perceptions in an agricultural region of the Ethiopian Highlands," *Weather and Climate Extremes*, vol. 29, Article ID 100263, 2020.

[69] A. Gebremichael, S. Quraishi, and G. Mamo, "Analysis of seasonal rainfall variability for agricultural water resource management in southern region, Ethiopia inter tropical convergence zone length of growing period," *Journal of Natural Sciences Research*, vol. 4, no. 11, pp. 56–80, 2014.

[70] G. M. Geremew, S. Mini, and A. Abegaz, "Spatiotemporal variability and trends in rainfall extremes in Enebsie Sar Midir district, northwest Ethiopia," *Model. Earth System Environment*, vol. 6, no. 2, pp. 1177–1187, 2020.

[71] M. Gedefaw, D. Yan, H. Wang, T. Qin, and K. Wang, "Analysis of the recent trends of two climate parameters over two eco-regions of Ethiopia," *Water (Switzerland)*, vol. 11, no. 1, p. 161, 2019.

[72] D. A. Tofu and M. Mengistu, "Observed time series trend analysis of climate variability and smallholder adoption of new agricultural technologies in west Shewa, Ethiopia," *Scientific African*, vol. 19, Article ID e01448, 2023.

[73] A. E. Harka, N. B. Jilo, and F. Behulu, "Spatial-temporal rainfall trend and variability assessment in the Upper Wabe Shebelle River Basin, Ethiopia: application of innovative trend analysis method," *Journal of Hydrology: Regional Studies*, vol. 37, Article ID 100915, 2021.

[74] A. Mekasha, K. Tesfaye, and A. J. Duncan, "Trends in daily observed temperature and precipitation extremes over three Ethiopian eco-environments," *International Journal of Climatology*, vol. 34, no. 6, pp. 1990–1999, 2014.